Clear-sky UV-B trends over northern midlatitudes derived from TOMS low-reflectivity footprint measurements

J. R. Ziemke[1]
Software Corporation of America, Beltsville, Maryland

S. Chandra
NASA Goddard Space Flight Center, Greenbelt, Maryland

C. Varotsos
University of Athens, Dept. of Applied Physics, Athens, Greece

Received _____; accepted _____

Submitted to *Journal of Geophysical Research*, 1999.

Short title: CLEAR-SKY UV-B TRENDS FROM TOMS MEASUREMENTS

[1]Also at NASA Goddard Space Flight Center, Greenbelt, Maryland.

Abstract. This study investigates the distribution of clear-sky ultraviolet-B (UV-B, wavelengths 290-320 nm) trends in northern midlatitudes using 1979-1991 Nimbus 7 total ozone mapping spectrometer (TOMS) version 7 low-reflectivity (R<0.2) total ozone footprint measurements. The incorporation of essentially cloud-free ozone data from TOMS provides a direct method for separating transient cloud effects from anthropogenic and other dynamical factors present in UV-B. This study has also included both National Oceanic and Atmospheric Administration (NOAA) microwave sounding unit channel 4 (MSU4) and National Centers for Environmental Prediction (NCEP) 500 hPa temperature (T500) fields in our trend models to improve UV-Index (UVI) trend statistics and to investigate the effects of interannual changes in UVI caused by synoptic-scale (horizontal wavelengths 4000-8000 km) and planetary-scale (horizontal wavelengths greater than 8000 km) dynamical events. Clear-sky UVI trends in the northern midlatitudes show large increases (exceeding 10 % per decade) and distinct regional variability especially during winter-spring months which can be attributed to topography and dynamical forcing effects. In the UV-important summer-autumn months, these trends are more uniformly distributed and still statistically significant, although smaller at around +2 to +3 % per decade. Specifically, during April largest increases in midlatitude UVI are seen to extend from near the dateline eastward across North America. In June months largest UVI increases occur over the east Asian continent with values around +5 to +6 % per decade. These increases in UVI over both the Pacific and Asian continent regions persist through summer into Autumn. In the the European sector, statistically significant increases in clear-sky UVI are found over central Europe with values around +2 to +3 % per decade and +8 to +9 % per decade during summer and winter-spring months, respectively. Over the nearby Mediterranean region these seasonal trends are around +2 to +3 and +5 to +6 % per decade.

1. Introduction

Solar Ultraviolet-B (UV-B) refers to UV radiation having wavelengths between 290 and 320 nm, and is strongly attenuated (especially the shorter wavelengths) by ozone in the stratosphere. Because ground-level UV-B and total ozone column (TOC) are inversely related [e.g., *Bojkov et al.*, 1995; *Fioletov et al.*, 1997], negative trends in TOC have produced measured increases (~4 to 12 % per decade) in surface zonal-mean UV-B in the midlatitudes of both hemispheres as shown by *Herman et al.* [1996] using 1979-1992 Nimbus 7 TOMS data. A more recent study by *Zerofos et al.* [1998] using ground-based data from Thessaloniki, Greece (41°N 23°E) shows increases in ground-level UV-B (at 305 nm) of around +10 % per decade for 1991-1997, a period coinciding with the declining phase of the 11-year solar cycle.

Ground-level UV-B depends on many variables besides just ozone and the effects from solar zenith angle (angle between the sun and the vertical), including transient cloud cover amount, surface albedo, aerosols (including pollution), and dynamical effects [e.g., *Hood and Zaff*, 1995; *Chandra et al.*, 1996; *McCormack and Hood*, 1997; *Hood et al.*, 1997; *Ziemke et al.*, 1997] making it difficult to isolate anthropogenic ozone depletion (and resulting surface UV-B increases) from non-anthropogenic causes [e.g., *Bruhl and Crutzen*, 1989; *Blumthaler and Ambach*, 1990; *Lubin and Jensen*, 1995; *Eck et al.*, 1995; *v. der Gathen et al*, 1995; *Rex et al.*, 1998]. The problem of isolating anthropogenic increases in surface UV-B becomes especially evident in regions where variations in TOC are strong. *Chandra et al.* [1996] suggested that in midlatitudes some of the observed trends in TOC may be manifestations of a relatively large interannual variability in TOC during winter-spring months and the length of the TOC time series. Because interannual variability in ozone is caused mainly by dynamical factors, such as the quasi-biennial oscillation (QBO), El Nino-southern oscillation (ENSO) and episodic medium-scale (4,000-8,000 km zonal wavelengths) and planetary-scale (wavelengths greater than 8000 km) waves [e.g., *Niu et al.*, 1992; *Hood and Zaff*, 1995; *Chandra et*

al., 1996; *McCormack and Hood*, 1997; *Ziemke et al.*, 1997], the trends in TOC and UV-B will likely vary significantly with latitude and longitude. *Chandra et al.* [1996] found that by using MSU4 deseasonalized temperature as an index of local dynamical variability in trend calculations, the large negative trends in midlatitude TOC are reduced in magnitude by 1 to 3 % per decade.

The purpose of our study is to investigate the distribution of clear-sky UV-Index (UVI) trends in the NH midlatitudes. UVI is a single number representing effective biological damage weighted over UV wavelengths [e.g., *Long et al.*, 1996]. Largest UVI occurs in the tropics under clear-sky conditions around equinox months with values exceeding 11. Smallest UVI (zero) may occur almost anywhere in the presence of dense cloudiness, but is ubiquitous in the high latitudes during winter. Our study determines clear-sky UVI using a direct method that incorporates only TOMS low-reflectivity (R<0.2) footprint measurements of TOC. The low-reflectivity scenes viewed by TOMS are essentially cloud-free and conceivably more accurate. This is because TOMS measures UV-wavelengths and cannot detect ozone lying below the tops of dense water vapor clouds. In order to obtain a total column measurement in the presence of a cloud, TOMS must assume a pre-determined amount of column ozone below the cloud top. Geophysically, the incorporation of essentially cloud-free ozone data from TOMS provides a straightforward method for removing transient cloud effects from anthropogenic and other dynamical factors present in UVI. In effort to further isolate anthropogenic effects in UVI trends, our study includes additional dynamical surrogates in regression trend models.

2. Data and Analyses

This study uses TOC data derived from Nimbus 7 TOMS version 7 observations from January 1979 through December 1991. We have chosen the 1979-1991 time period because after 1991 and until the failure of the TOMS instrument in May 1993, TOC

values in midlatitudes were affected by the Mt Pinatubo eruption [e.g., *Gleason et al.*, 1993]. In this respect, *Chandra* [1993] and *Randel and Cobb* [1994] suggested that the inclusion of the post-Pinatubo period causes TOC trends to be more negative by 0.2 to 1.2 % per decade. We note that more current TOMS measurements exist for studying long-term variability including Meteor 3 TOMS (1991-1994) and Earth Probe (EP) TOMS data for late July 1996 to the present. However, because of instrument calibration differences, derived trends in either TOC or surface UV-B are less certain when these different instruments are combined to obtain a longer time record. For this reason and also because the 1979-1991 time period corresponds to one complete peak-to-peak cycle in solar UV (important for regression analysis), we have opted to include only the Nimbus 7 data.

To derive trends in clear-sky UVI we have used daily level-2 TOMS footprint data filtered for low-reflectivity (R<0.2) scenes and gridded to a horizontal resolution of 1° in latitude and 1.25° in longitude, similar to the standard level-3 TOMS gridded TOC product (currently, standard level-3 TOC data are available via World Wide Web at http://jwocky.gsfc.nasa.gov). We note that for individual R<0.2 TOMS ozone footprint measurements, below-cloud column amount from the version 7 algorithm is at most around 1-2 Dobson units (DU). Clear-sky UVI in our study was derived directly from R<0.2 TOMS total ozone measurements using the parameterization scheme of *Austin et al.* [1994]. For completeness in our study, we restate the UVI parameterization scheme of *Austin et al.* [1994] which is

$$\mathrm{UVI} = \cos\theta \times e^{[A+Bm\Omega+Cm+D(m\Omega)^2+Em^2]}, \qquad (1)$$

where θ=solar zenith angle, m=ratio of the slant path of the solar beam to the vertical ($\sim 1/\cos\theta$), Ω = TOC in DU, A=3.874, B=-3.927E-3, C=-0.636, D=1.525E-6, and E=0.1183.

Prior to our trend analyses, all data were averaged monthly and binned to a

5°× 5°gridding. For computing regional trends, data were averaged over a larger grid size. To define the Mediterranean region we considered the latitude band 35-45°N and longitudes 0-30°E, and for Central Europe a 5°× 15°region centered at 50°N, 15°E.

UVI trends were calculated using an extended linear regression model similar to *Ziemke et al.* [1997] (t = 0, 1, ..., 155, corresponding to Jan79-Dec91):

$$\mathrm{UVI}(t) = A(t) + B(t)t + C(t)\mathrm{QBO}(t) + D(t)\mathrm{S}(t)$$

$$+E(t)\mathrm{P}(t) + \mathrm{R}(t), \qquad (2)$$

where $A(t)$ represents the 12-month seasonal fit, $B(t)$ is the 12-month seasonal trend coefficient, R(t) represents the residual error time series, and $C(t)$, $D(t)$, and $E(t)$ are 12-month coefficients corresponding to UV-driving time series QBO(t) (30 hPa quasi-biennial oscillation zonal winds), S(t) (F10.7 solar UV proxy), and an optional proxy P(t). For S(t) in (2), Ottawa 10.7 cm solar flux (F10.7) monthly time series was incorporated. For P(t) we have used deseasonalized and linearly detrended temperature data from the U.S. National Center for Environmental Prediction (NCEP) and microwave sounding unit channel 4 (MSU4) temperature data from National Oceanic and Atmospheric Administration (NOAA). Temperature analyses from NCEP used in this study represent the low to midtroposphere centered at 500 hPa. Temperatures from MSU4 are weighted mean values centered at around 90 hPa in the stratosphere (half vertical weighting response close to 40 and 150 hPa).

Trends derived from (2) also include additional 1 % per decade local measurement uncertainties present in version 7 TOMS TOC, which for UVI translates to 1.0 to 1.3 % per decade throughout midlatitudes (largest errors in winter months). For simplicity we have opted to include additional 1.3 % per decade uncertainties in derived UVI trends everywhere in our analyses.

In winter months the incidences of snow and ice, particularly in the higher latitudes, degrade the R<0.2 TOC data set as there are fewer low-reflectivity scenes viewed

by TOMS. For our study we present results for the higher latitudes only in months (i.e., late spring into autumn) where there is a sufficient number of R<0.2 footprint measurements for analysis.

3. Discussion and Results

Figure 1 compares deseasonalized time series of clear-sky UVI (solid) and MSU4 brightness temperature (dotted) over central Europe (top) and the Mediterranean region (bottom). For purposes of comparison with background UVI amounts, climatological values of clear-sky UVI for these two regions are provided in Table 1.

The UVI and MSU4 time series in Figure 1 show a distinct negative correlation which is caused primarily by interannual changes in dynamical transport of stratospheric ozone [e.g., *Chandra et al.*, 1996; *Ziemke et al.*, 1997]. Also plotted in Figure 1 are simple regression line fits for both UVI time series, indicating statistically significant increases in UVI of around 0.10 and 0.13 per decade (3.2 and 2.7 % per decade) over central Europe and the Mediterranean region, respectively. We note that the positive trends in UVI are associated with negative trends in TOC, and coincide with negative trends in MSU4 temperatures (line fits not shown in Figure 1). This implies stratospheric radiative effects (depletion of ozone reduces temperature) and/or decadal changes in dynamical transport. While radiative effects will be present on such a long time scale, there is evidence that decadal changes in dynamical transport have had a role in observed negative trends in TOC over northern-hemisphere (NH) midlatitudes [e.g., *Hood and Zaff*, 1995; *Chandra et al.*, 1996; *Hood et al.*, 1997; *Ziemke et al.*, 1997].

A comparison of UVI temperature sensitivities (E(t) coefficients in (2)) for both of the MSU4 and T500 trend models is shown in Figure 2 for central Europe (top) and the Mediterranean (bottom). For central Europe and the Mediterranean region during the important summer months a 1K increase in T500 (associated mostly with synoptic-scale events) coincides with increases of 0.1 to 0.2 in clear-sky surface UVI. In

comparison, a 1K increase in MSU4 temperature is associated with decreases in UVI of around 0.3. Despite both proxies showing statistically significant sensitivies with UVI (positive relation for T500, negative for MSU4) especially during the important NH summer months, we have opted to use the MSU4 proxy for the remainder of our study because of better statistics throughout NH midlatitudes.

Figure 3 shows UVI trends for central Europe (top) and the Mediterranean region (bottom) as derived from a standard regression model (dotted) and MSU4 model (solid). (The standard trend model is defined without the optional proxy P(t) term in (2).) In central Europe (Figure 3, top) both models yield similar trends but with generally smaller 2-sigma trend uncertainties using MSU4. The UVI trends over central Europe reach +9 % per decade around March and +2 to +3 % per decade in summer months. In the Mediterranean region (Figure 3, bottom) UVI trends are similar during summer, but smaller (around +5 to +6 % per decade) in winter-spring months. The inclusion of MSU4 data in trend analyses for the Mediterranean region results in shifts of several % per decade including the appearance of statistically significant trends around November-December when compared to the standard model.

Our study has analyzed clear-sky UVI trends throughout NH midlatitudes. Figure 4 shows monthly UVI trends plotted zonally (west to east) around the Earth at fixed latitude 40°N. During winter months trends show a marked longitudinal pattern, attributed to topography and dynamical transport forcing effects [e.g., *Hood and Zaff*, 1995]. During summer-autumn months, trends are smaller (+2 to +3 % per decade) but still statistically significant throughout most of the domain shown. For completeness, Figure 5 shows the horizontal distribution of UVI trends for the important spring and summer months of April (top) and June (bottom). In April, largest increases in UVI extend over midlatitudes from around the dateline eastward across North America. In June a shift occurs with largest UVI increases (+5 to +6 % per decade) over the east Asian continent. The increases in UVI over both the Pacific and east Asian regions

persist througout summer into Autumn as shown in Figure 6 for August (top) and October (bottom) months. The increases in UVI over the region of east Asia from summer into Autumn are statistically significant because of dynamical planetary wave structure present in the MSU4 data.

4. Summary

This study has investigated regional clear-sky UVI trends in NH midlatitudes using a direct approach that incorporates only TOMS low-reflectivity (R<0.2) footprint measurements for 1979-1991. Because TOMS measures backscattered UV radiation it cannot detect ozone lying below dense water vapor clouds and must place a pre-determined amount of column ozone below cloud tops. Low-reflectivity scenes conceivably provide the best values for TOMS TOC in regions primarily free of snow and ice, as in this study. Geophysically, the incorporation of essentially cloud-free TOC measurements from TOMS provides a straightforward approach for separating transient cloud effects from anthropogenic and other dynamical factors present in UVI. In effort to reduce dynamical influences in UVI trends, our study has also included additional dynamical surrogates in regression trend models.

Results indicate that clear-sky UVI trends in the northern midlatitudes exhibit large increases (exceeding 10 % per decade) and distinct regional variability especially during winter-spring months which can be attributed to topography and dynamical forcing effects. In summer-autumn months, these trends are more uniformly distributed and smaller at around +2 to +3 % per decade. For the UV-important spring-autumn months our study indicates considerable seasonal changes in the distribution of UVI trends. During spring, largest increases in UVI occur over the Pacific extending eastward across the North American continent. In summer, largest UVI increases occur over the east Asian continent with values around +5 to +6 % per decade. The increases in UVI over both the Pacific and Asian continent regions persist throughout summer into

Autumn. Over the European sector, results indicate statistically significant increases in clear-sky UVI of around +2 to +3 % per decade and +8 to +9 % per decade over central Europe during summer and winter-spring months, respectively. In the nearby Mediterranean region these trends are around +2 to +3 % per decade in summer and +5 to +6 % per decade during winter-spring.

Both MSU4 (i.e., lower stratosphere) and T500 (low to midtroposphere) temperature fields were included as additional dynamical proxies in clear-sky UVI trend models to improve trend statistics for UVI. In all seasons trend statistics improved because of a sensitivity of UVI to episodic dynamical events. Sensitivity coefficients indicated that in central Europe and the Mediterranean region during the important summer months a +1K interannual change in T500 (associated mostly with interannual changes in synoptic-scale events) was found to be associated on average with a +0.1 to +0.2 change in clear-sky surface UVI. In contrast, a +1K change in lower stratospheric temperature from MSU4 indicated changes in UVI of around -0.3.

Acknowledgments. We wish to thank members of the NASA TOMS Nimbus Experiment and Information Processing Teams for providing the version 7 TOMS ozone data. We also greatly thank both NOAA and NCEP for providing the extensive temperature data used in this study.

References

Austin J., B.R. Barwell, S. J. Cox, P. A. Hughes, J. R. Knight, G.Ross, P. Sinclair, and A. R. Webb, The diagnosis and forecast of clearsky ultraviolet levels at the Earth's surface, Meteorol. Apps., 1, 321-336, 1994.

Blumthaler, M. and W. Ambach, Indication of increasing solar ultraviolet-B radiation flux in alpine regions, *Science, 248*, 206-208, 1990.

Bojkov R. D., V. E. Fioletov and S. B. Diaz, The relationship between solar UV irradiance and total ozone from observations over southern Argentina, *Geophys. Res. Lett., 22*, 1249-1252, 1995.

Bruhl, C. And P. J. Crutzen, On the disproportionate role of tropospheric ozone as a filter against solar UV-B radiation, *Geophys. Res. Lett., 16*, 703-706, 1989.

Chandra, S., Changes in stratospheric ozone and temperature due to the eruption of Mt. Pinatubo, *Geophys. Res. Lett., 20*, 33-36, 1993.

Chandra, S. and R. S. Stolarski, Recent trends in stratospheric total ozone: Implications of dynamical and El Chichon perturbations, *Geophys. Res. Lett., 18*, 2277-2281, 1991.

Chandra, S., C. Varotsos, and L. E. Flynn, The mid-latitude total ozone trends in the northern hemisphere, *Geophys. Res. Lett., 23*, 5, 555-558, 1996.

Eck, T. F., P. K. Barthia, and J.B. Kerr, Satellite estimation of spectral UVB irradiance using TOMS derived ozone and reflectivity, *Geophys. Res. Lett., 22*, 611-614, 1995.

Fioletov V., J. Kerr and D. Wardle, The relationship between total ozone and spectral UV irradiance from Brewer observations and its use for derivation of total ozone from UV measurements, Geophys.Res.Lett., 24, 2997-3000, 1997.

Gleason, J., et al., Record low global ozone in 1992, *Science, 260*, 523-525, 1993.

Herman, J. R., P. K. Bhartia, J. Ziemke, Z. Ahmad and D. Larko, UV-B increases (1979-1992) from decreases in total ozone, *Geophys. Res. Lett., 23*, 2117-2120, 1996.

Hood, L. L., and D. A. Zaff, Lower stratospheric stationary waves and the longitude dependence of ozone trends in winter, *J. Geophys. Res., 100*, 25,791-25,800, 1995.

Hood, L. L., J. P. McCormack, and K. Labitzke, An investigation of dynamical contributions

to midlatitude ozone trends in winter, *J. Geophys. Res., 102*, 13,079-13,093, 1997.

Long, C. S., A. J. Miller, H.-T. Lee, J. D. Wild, R. C. Przywarty, and D. Hufford, Ultraviolet index forecasts issued by the National Weather Service, *Bull. Am. Meteorol. Soc., 77*, 729–748, 1996.

Lubin, D., and E. H. Jensen, Effects of clouds and stratospheric ozone depletion on ultraviolet radiation changes, Nature, 377, 710-713, 1995.

McCormack, J. P., and L. L. Hood, Modeling the spatial distribution of total ozone in northern hemisphere winter: 1979-1991, *J. Geophys. Res., 102*, 13,711-13,717, 1997.

Niu, X., J. E. Frederick, M. L. Stein, and G. C. Tiao, Trends in column ozone based on TOMS data: Dependence on month, latitude, and longitude, J. Geophys. Res., 97, 14, 661-669, 1992.

Randel W. J., and J. B. Cobb, Coherent variations of monthly mean total ozone and lower stratospheric temperature, *J. Geophys. Res., 99*, 5433-5447, 1994.

Rex M., P. von der Gathen, N. R. P. Harris, D. Lucic, B. M. Knudsen, G. O. Braathen, S. J. Reid, H. De Backer, H Claude, R. Fabian, H. Fast, M. Gil, E. Kyr, I. S. Mikkelsen, M. Rummukainen, H.G. Smit, J. Sthelin, C. Varotsos, I. Zaitcev: In-situ measurements of stratospheric ozone depletion rates in the Arctic Winter 1991/92: A Lagrangian Approach. *J. Geophys. Res., 103*, 5843-5853, 1998.

v. der Gathen P., M. Rex, N. R. P. Harris, D. Lucic, B. M. Knudsen, G. O. Braathen, H. De Backer, R. Fabian, H. Fast, M. Gil, E. Kyr, I. S. Mikkelsen, M. Rummukainen, J. Sthelin and C. Varotsos, Observational evidence for chemical ozone depletion over the Arctic in winter 1991-92. *Nature, 375*, 131-134, 1995.

Zerefos, C., C. Meleti, D. Balis, K. Tourpali, and A. F. Bais, Quasibiennial and longer-term changes in clear-sky UV-B solar irradiance, *Geophys. Res. Lett., 25* 4345-4348, 1998.

Ziemke, J. R., S. Chandra, and R. D. McPeters, Dynamical proxies of column ozone with applications to global trend models, *J. Geophys. Res., 102*, 6117-6129, 1997.

This manuscript was prepared with the AGU LaTeX macros v3.1.

Figure 1. Deseasonalized clear-sky UVI (solid) and deseasonalized MSU4 brightness temperature (dotted) time series over central Europe (top) and the Mediterranean region (bottom). Central Europe is defined by a 5°× 15°region centered at 50°N, 15°E. Also shown are regression line fits for both UVI time series. For central Europe, the linear trend is 0.104 ±0.055 (2σ), or equivalently 3.15 ±1.67 % per decade. For the Mediterranean region, the trend is 0.129 ±0.059(2σ), or equivalently 2.67 ±1.22 % per decade.

Figure 2. Monthly sensitivity coefficients (E(t) in (2) with units K^{-1}) for clear-sky UVI derived from the MSU4 model (solid) and T500 model (dashed) over central Europe (top) and the Mediterranean region (bottom). Central Europe is defined by a 5°× 15°region centered at 50°N, 15°E. Also shown are ±2σ uncertainty bars.

Figure 3. Monthly linear trends in clear-sky UVI for the standard model (dashed) and MSU4 model (solid) over central Europe (top) and the Mediterranean region (bottom). Central Europe is defined by a 5°× 15°region centered at 50°N, 15°E. Also shown are ±2σ uncertainty bars.

Figure 4. Trends in clear-sky UVI as a function of longitude and month at fixed latitude 40°N. Shaded regions indicate trends that are not different from zero at the 2σ level.

Figure 5. Latitude versus longitude 1979-1991 regression model trends in northern hemisphere clear-sky UVI. Units: Percent per decade. Shading indicates trends not different from zero at the 2σ level. (top) April. (bottom) June.

Figure 6. Latitude versus longitude 1979-1991 regression model trends in northern hemisphere clear-sky UVI. Units: Percent per decade. Shading indicates trends not different from zero at the 2σ level. (top) August. (bottom) October.

Table 1. Monthly climatology (1979-1991) of clear-sky UVI for central Europe and Mediterranean regions.

Region	Jan.	Feb.	March	April	May	June	July	Aug.	Sept.	Oct.	Nov.	Dec.	Avg.
Cent. Eur.	0.6	0.7	1.4	3.0	4.9	6.3	6.8	6.4	5.0	2.9	1.2	0.6	3.3
Medit.	1.3	1.7	3.0	4.9	6.7	8.0	8.6	8.2	6.8	4.7	2.6	1.5	4.8

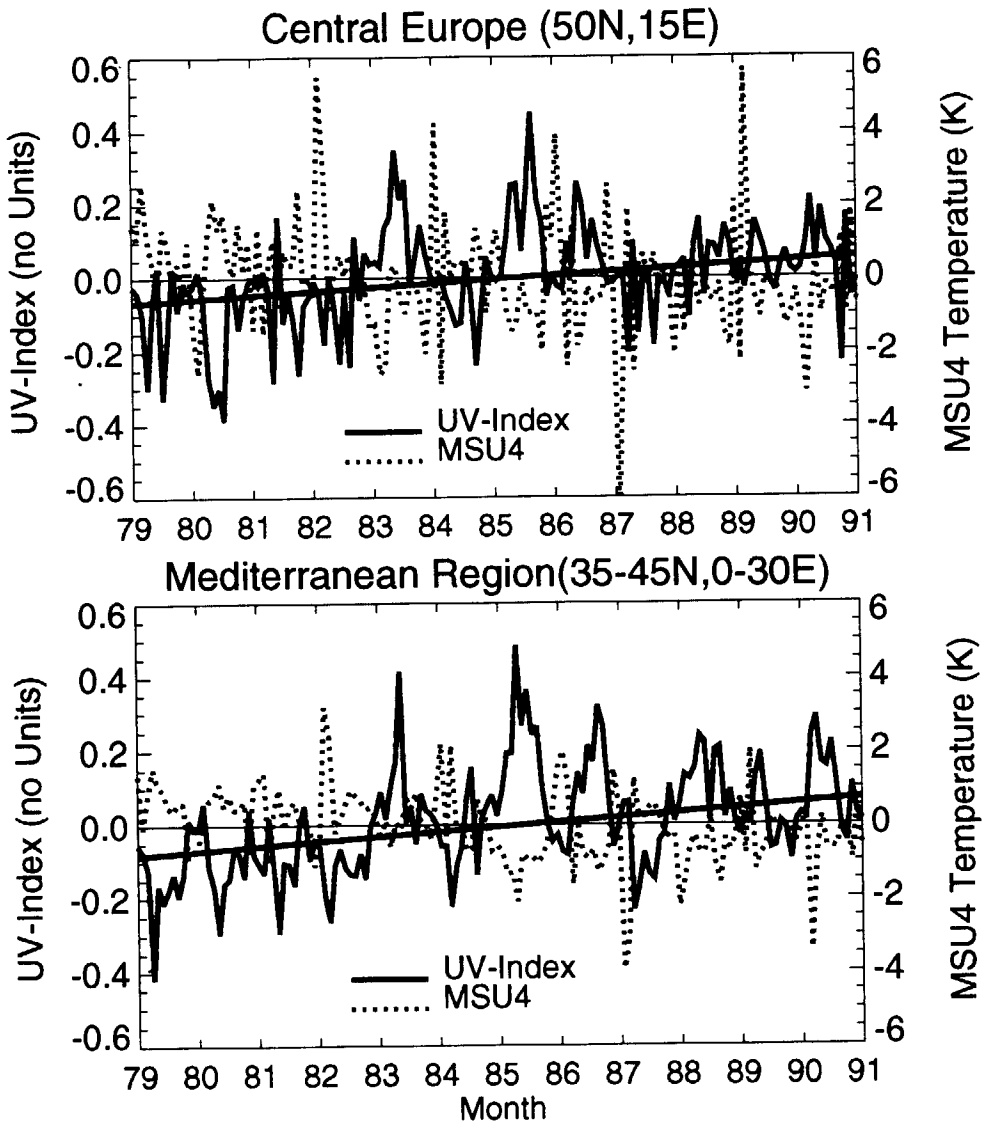
Central Europe (50N,15E)
UV-Index (no Units)
MSU4 Temperature (K)
0.6
0.4
0.2
0.0
-0.2
-0.4
-0.6
6
4
2
0
-2
-4
-6
UV-Index
MSU4
79 80 81 82 83 84 85 86 87 88 89 90 91
Mediterranean Region(35-45N,0-30E)
UV-Index (no Units)
MSU4 Temperature (K)
UV-Index
MSU4
79 80 81 82 83 84 85 86 87 88 89 90 91
Month

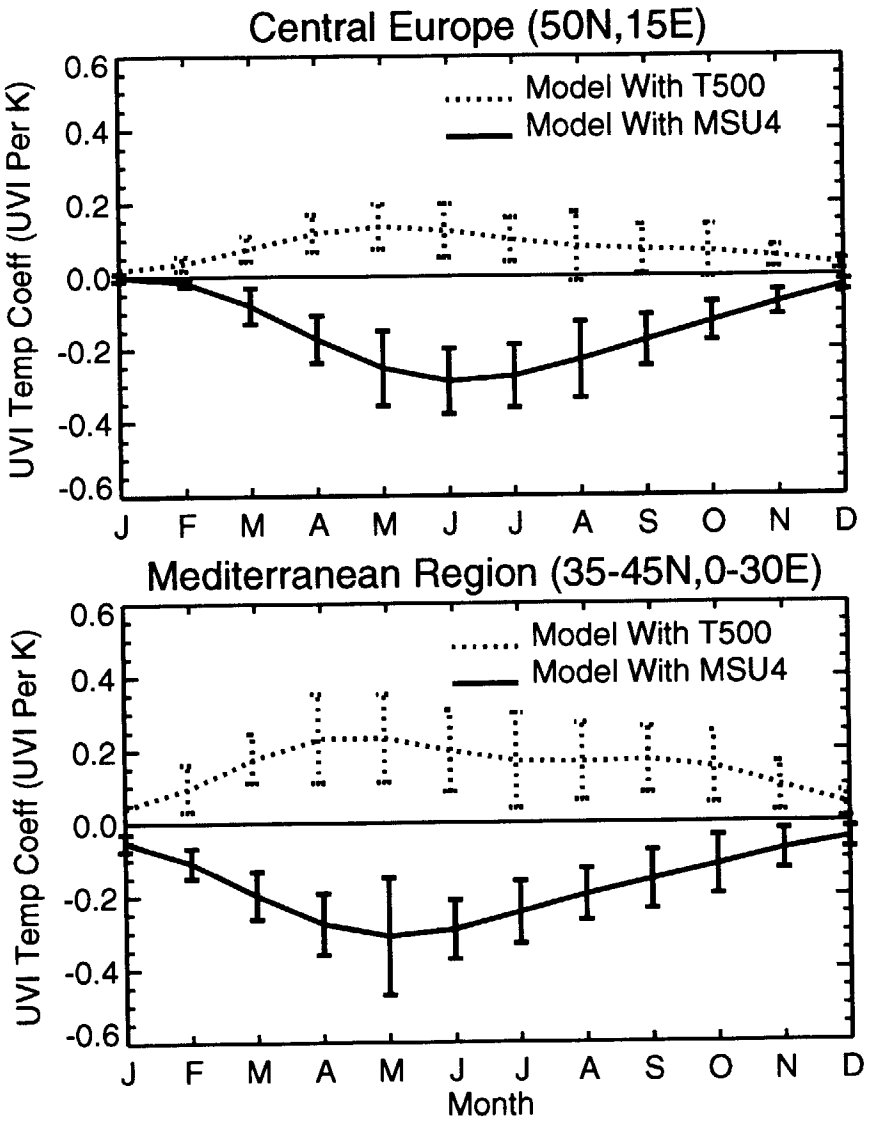
Central Europe (50N,15E)
Model With T500
Model With MSU4
UVI Temp Coeff (UVI Per K)
0.6
0.4
0.2
0.0
-0.2
-0.4
-0.6
J F M A M J J A S O N D
Mediterranean Region (35-45N,0-30E)
Model With T500
Model With MSU4
UVI Temp Coeff (UVI Per K)
0.6
0.4
0.2
0.0
-0.2
-0.4
-0.6
J F M A M J J A S O N D
Month

F2

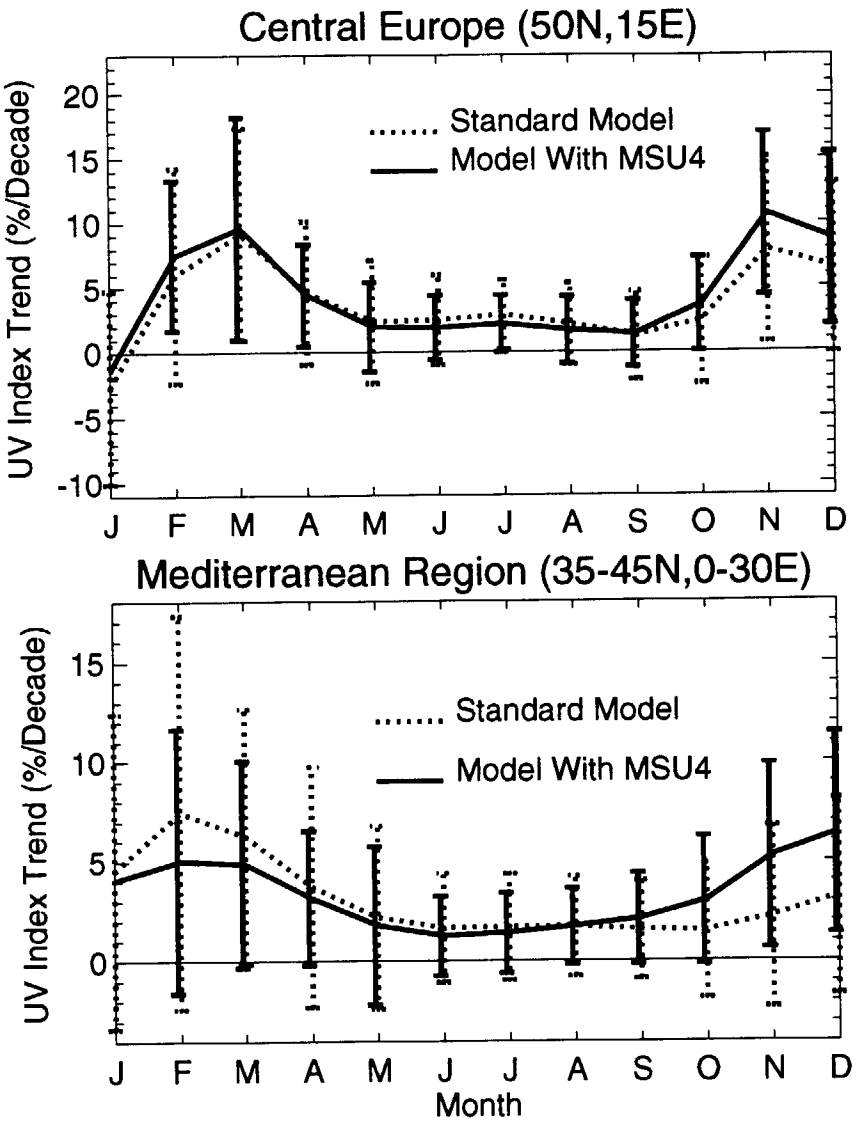
Central Europe (50N,15E)
UV Index Trend (%/Decade)
20
15
10
5
0
-5
-10
Standard Model
Model With MSU4
J F M A M J J A S O N D
Mediterranean Region (35-45N,0-30E)
UV Index Trend (%/Decade)
15
10
5
0
Standard Model
Model With MSU4
J F M A M J J A S O N D
Month

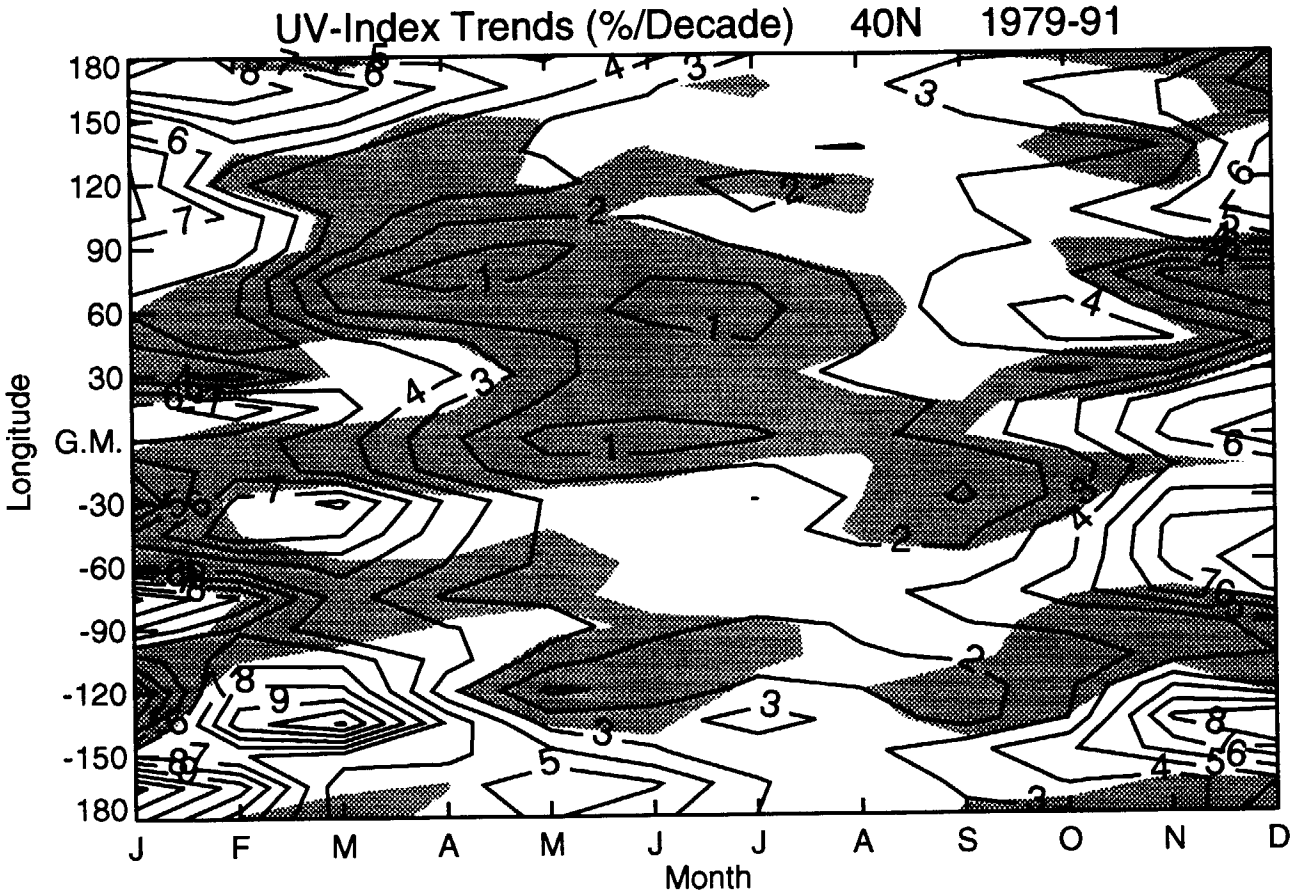
UV-Index Trends (%/Decade) 40N 1979-91
Longitude
180
150
120
90
60
30
G.M.
-30
-60
-90
-120
-150
180
J
F
M
A
M
J
J
A
S
O
N
D
Month

F4

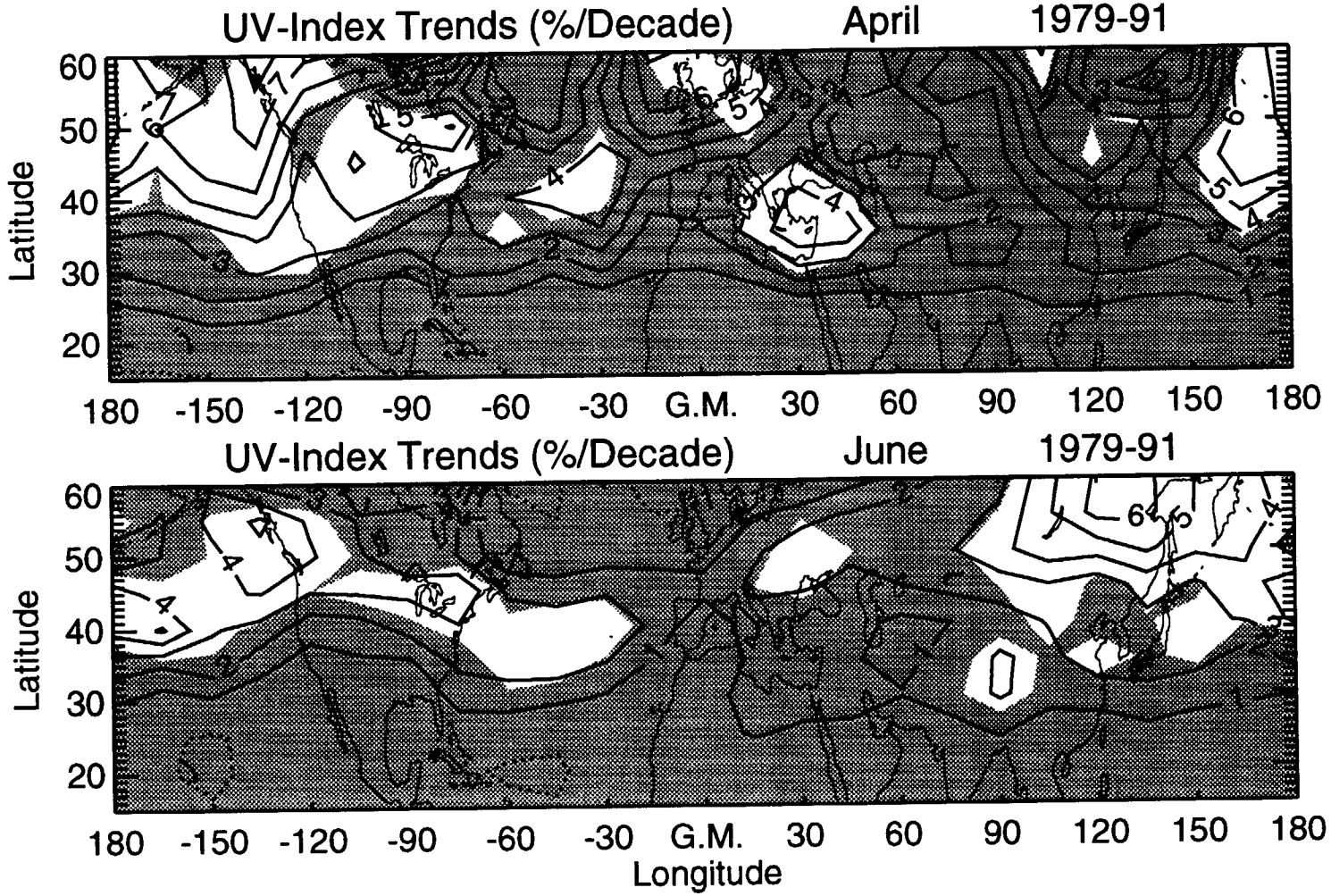
UV-Index Trends (%/Decade) April 1979-91
Latitude
60
50
40
30
20
180 -150 -120 -90 -60 -30 G.M. 30 60 90 120 150 180
UV-Index Trends (%/Decade) June 1979-91
Latitude
60
50
40
30
20
180 -150 -120 -90 -60 -30 G.M. 30 60 90 120 150 180
Longitude

51

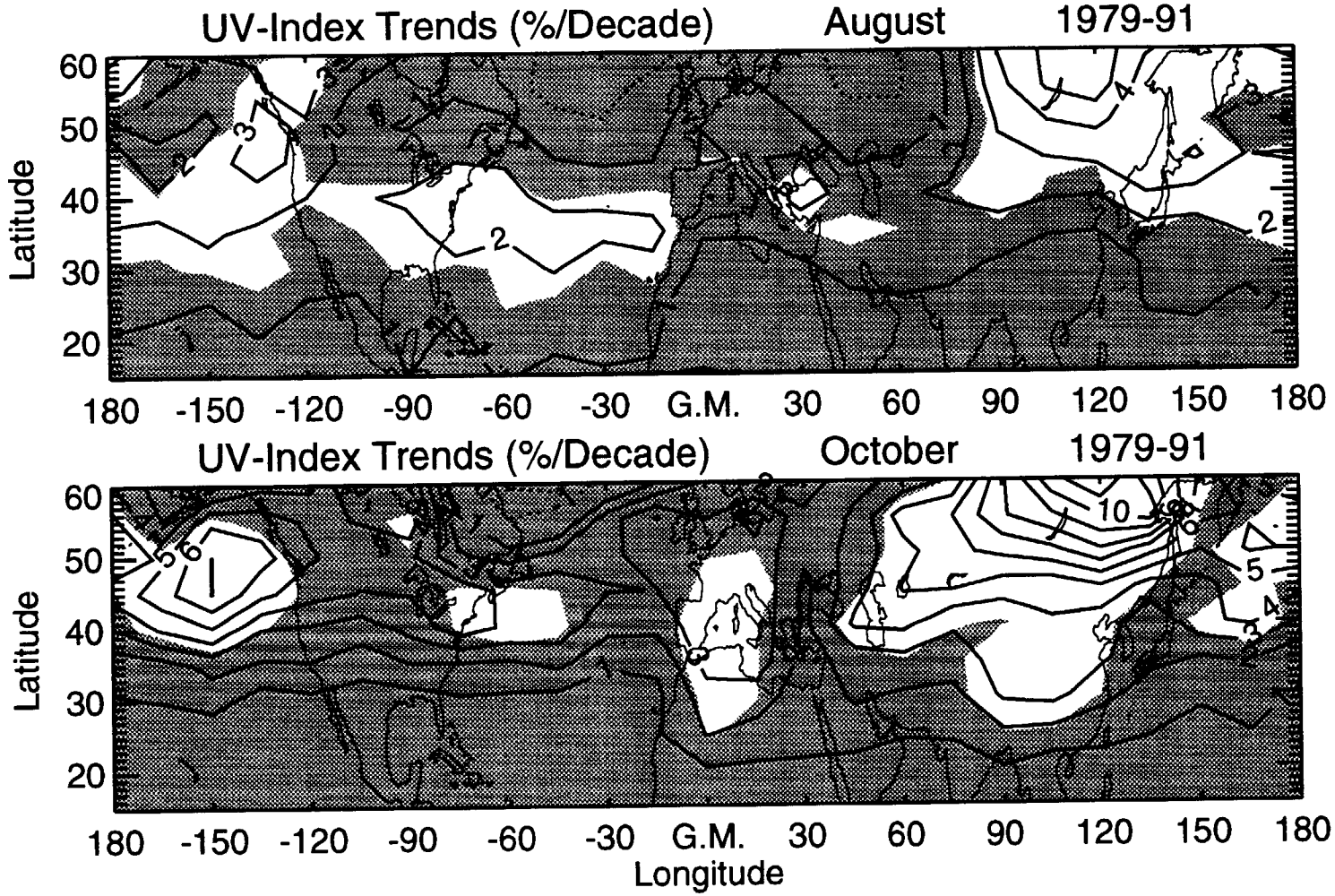
UV-Index Trends (%/Decade) August 1979-91
Latitude
60
50
40
30
20
180 -150 -120 -90 -60 -30 G.M. 30 60 90 120 150 180
UV-Index Trends (%/Decade) October 1979-91
Latitude
60
50
40
30
20
180 -150 -120 -90 -60 -30 G.M. 30 60 90 120 150 180
Longitude